J Toxicol Pathol 2018; 31: 73–80

Short Communication

Size-dependent acute toxicity of silver nanoparticles in mice

Young-Man Cho[1]*, Yasuko Mizuta[1], Jun-ichi Akagi[1], Takeshi Toyoda[1], Mizuki Sone[1], and Kumiko Ogawa[1]

[1] Division of Pathology, Biological Safety Research Center, National Institute of Health Sciences, 1-18-1 Kamiyoga, Setagaya-ku, Tokyo 158-8501, Japan

Abstract: In this study, we aimed to evaluate changes in the acute toxicity of intraperitoneally administered silver nanoparticles (AgNPs) of varying sizes in BALB/c mice. Seven-week-old female BALB/c mice were intraperitoneally administered AgNPs measuring 10, 60, or 100 nm in diameter (0.2 mg/mouse) and then sacrificed 1, 3, or 6 h after treatment. In mice administered 10 nm AgNPs, reduced activity and piloerection were observed at 5 h post administration, and lowered body temperature was observed at 6 h post administration, with histopathological changes of congestion, vacuolation, single cell necrosis, and focal necrosis in the liver; congestion in the spleen; and apoptosis in the thymus cortex. These histopathological changes were not evident following administration of either 60 or 100 nm AgNPs. These results suggested that smaller AgNPs, e.g., those measuring 10 nm in diameter, had higher acute toxicity in mice. (DOI: 10.1293/tox.2017-0043; J Toxicol Pathol 2018; 31: 73–80)

Key words: silver nanoparticles, size dependence, acute toxicity, intraperitoneal administration, BALB/c mice

Nanotechnology is rapidly developing, and nanoparticles (NPs) can now be produced and utilized in a wide array of end-user products owing to their size-related physicochemical properties[1]. Silver NPs (AgNPs) are commonly used in consumer products, including food supplements, plastic food containers, coatings on medical devices, water disinfectants, air filters, electronic appliances, odor-resistant textile fabrics, and cosmetics products, such as deodorants, due to their antimicrobial properties[1–5]. AgNPs have become attractive materials for application as effective drug delivery vehicles and cancer therapeutic agents[6].

In vitro, AgNPs induce cytotoxicity and genotoxicity in human normal bronchial epithelial cells[7, 8]. Moreover, AgNPs can be taken up by human skin keratinocytes and become internalized inside the cells owing to the size and shape of the NPs[9]. Further studies are needed to elucidate the contribution of particle size and surface area to NP dissolution by shedding of Ag ions, which are thought to contribute to AgNP toxicity[10]. Many studies on toxicity *in vivo* have been also reported; however, most of these studies have employed administration routes such as inhalation and oral and transdermal delivery and have used particles with only one size or with a wide range of sizes. In a 13-week inhalation study in rats, the lung and liver were found to be AgNP-target organs, and the results showed in chronic alveolar inflammation and bile duct hyperplasia, respectively[11]. In a 13-week oral toxicity study in rats, the liver was the target organ, and the results showed bile duct hyperplasia[12]. In an acute dermal study in rats and rabbits, there were no abnormal signs or corrosion reactions on the skin[13]. Although reports of human exposure via several routes have been rapidly increasing owing to increases in the manufacture and utilization of AgNPs, very few reports have described the acute toxicity associated with different sizes of AgNPs[14].

In our preliminary study performed to evaluate immunotoxicity, the same amount of AgNPs with diameters of 10, 60, or 100 nm were intraperitoneally administered into female BACL/c mice. Unexpectedly, all 10 mice administered 10 nm AgNPs were found dead or moribund within 24 h, although mice in all other groups showed no clinical symptoms. The purpose of the present study was to evaluate the histopathological and biochemical changes associated with the acute toxicity of intraperitoneally administered AgNPs of varying sizes in BALB/c mice.

Six-week-old female BALB/c mice were purchased from Japan SLC (Hamamatsu, Shizuoka, Japan) and acclimated for 1 week prior to initiation of the experiment. Mice were maintained in a room with a barrier system under the following conditions: temperature of 24 ± 1°C, relative humidity of 55 ± 5%, ventilation frequency of 18 times/h, and 12-h light/dark cycle. The animals were housed at 5 mice per plastic cage, with sterilized soft wood chips (Sankyo Laboratory Service, Tokyo, Japan) for bedding, in a specific pathogen-free animal facility. All animals were allowed free access to tap water and a commercial Mouse

Received: 14 July 2017, Accepted: 22 October 2017
Published online in J-STAGE: 19 November 2017
*Corresponding author: Y-M Cho (e-mail: ymcho@nihs.go.jp)

Flat (MF) diet (Oriental Yeast Co., Ltd, Tokyo, Japan) *ad libitum*. The mice were maintained in the National Institute of Health Sciences, according to the Institutional Regulations for Animal Experiments. The regulations included the best considerations for animal welfare and good practice of animal handling contributing to the replacement, refinement, and reduction of animal testing (3Rs).

Three different sizes (10, 60, and 100 nm in diameter) of spherical AgNPs (BioPure Silver Nanoparticles) were purchased from nanoComposix (San Diego, CA, USA). The citrate-stabilized particles were supplied as 1.0-mg/mL suspensions in 2 mM sodium citrate. BioPure AgNPs were chosen because they have a narrow particle size distribution and are guaranteed to be sterilized with an endotoxin level lower than 2.5 EU/mL. Baseline information about the material characteristics of the AgNPs purchased for the present study, including endotoxin levels, hydrodynamic size, size distribution by dynamic light scattering, and transmission electron microscopy (TEM; JEOL 1010), zeta potential (Malvern Zetasizer Nano ZS), silver concentration by inductively coupled plasma mass spectrometry (Thermo Fisher XSeries 2 ICP-MS), and UV-visible spectra (Agilent 8453 UV-Visible Spectrometer) were provided by the supplier (Table 1). AgNPs particles of different size have different colors: dark brown, 10 nm; gray to black, 60 nm; and light gray, 100 nm. Trisodium citrate dihydrate was purchased from Wako Pure Chemical Industries, Ltd. (Osaka, Japan).

In our preliminary study, all mice (7-week-old female BALB/c mice, 5 mice/group) were intraperitoneally injected with 10 nm AgNPs (0.3-mL dispersion in 2 mM citrate buffer, 0.2 mg/mouse) with or without ovalbumin (OVA) and were found dead or moribund within 24 h. In contrast, all mice given 60 or 100 nm AgNPs showed no clinical symptoms.

Mice (body weight [bw]: 16.3 − 20.2 g) were divided in 4 groups: 10 nm (n=15), 60 nm (n=15), 100 nm (n=15), and control (n=5). They were intraperitoneally injected with either 0.3 mL of an AgNP dispersion (0.2 mg AgNP/mouse, 9.9 − 12.3 mg/kg bw) or vehicle control (2 mM citrate). Food and water were available *ad libitum*. Clinical signs and mortality were carefully checked frequently. At 1, 3, and 6 h after treatment, animals (n=5 mice/group/time point) were anesthetized with isoflurane (Mylan Inc., Tokyo, Japan), and blood samples were collected from the abdominal aorta for serum biochemistry. Sacrifice and blood sample collection from the animals in the control group were conducted at 6 h only. Animals were then euthanized by exsanguination from the abdominal aorta. Rectal temperatures were measured with a rectal thermometer (BAT-7001H, Physitemp Instruments Inc., Clifton, NJ, USA) just before injection and at 1, 3, and 6 h. The protocol was approved by the Animal Care and Utilization Committee of the National Institute of Health Sciences (Tokyo, Japan).

Serum biochemistry was analyzed at Oriental Yeast Co., Ltd. (Tokyo, Japan), using sera frozen after centrifugation of whole blood (1,000 × *g*, 10 min). The following parameters were analyzed: total protein (TP), albumin (ALB), ALB/globulin ratio (A/G), urea nitrogen (BUN), creatinine (Cre), sodium (Na), potassium (K), chlorine (Cl), calcium (Ca), inorganic phosphorus (IP), aspartate aminotransferase (AST), alanine aminotransferase (ALT), alkaline phosphatase (ALP), gamma-glutamyl transpeptidase (γGTP), triglyceride (TG), total bilirubin (Bil), and glucose.

All animals were subjected to complete necropsy. The brain, thymus, lungs, heart, spleen, liver, kidneys, pancreas, and mesenteric lymph nodes were excised. All organs and tissues as well as the remaining body parts were fixed in 10% buffered formalin. Paraffin-embedded tissue sections of all organs/tissues were routinely prepared and stained with hematoxylin and eosin (HE).

Liver tissues were embedded in paraffin, sectioned to 4-μm thickness, and subjected to immunohistochemistry using a Histofine Simple Stain Kit (Nichirei Corp, Tokyo, Japan) with 3,3′-diaminobenzidine/H_2O_2 as a chromogen. Anti-Ki-67 rabbit monoclonal antibodies (clone SP6, 1:1000; Abcam, Cambridge, CA, USA) were used as primary antibodies. Antigen retrieval was performed in an autoclave for 10 min at 121°C in 10 mM citrate buffer (pH 6.0).

Variances in the data for serum biochemistry, rectal temperatures, serum biochemistry, and immunohistochemistry were checked for homogeneity by Bartlett's procedure. When the data were homogeneous, one-way analysis of variance was applied. In heterogeneous cases, the Kruskal-Wallis test was used. When statistically significant differences were indicated, Dunnett's multiple test was employed for comparisons between control and treated groups. For

Table 1. Characteristics of the Silver Nanoparticles Per Particle Solution

	10 nm AgNP	60 nm AgNP	100 nm AgNP
Lot No.	DMW0198	DMW0164	DMW0120
Diameter (nm)	9.6 ± 2	59.8 ± 6.2	104.3 ± 12.6
Coefficient of variation (%)	20.4	10.3	12.1
Particle concentration (mL^{-1})	2.2×10^{14}	9.1×10^{11}	1.7×10^{11}
Surface area (m^2/g)	55.1	9.4	5.3
Mass concentration (mg/mL)	1.07	1.07	1.05
Endotoxin concentration (EU/mL)	< 5	< 2.5	< 2.5
Zeta potential (mV)	−39.4	−46.5	−49.3
pH of solution	7.7	7.5	7.3
Hydrodynamic diameter (nm)	13.3	65.8	107
Silver purity (%)	99.99	99.99	99.99

analysis of histopathological findings, Fisher's exact probability test (two-tailed) was applied. Differences with *P* values of less than 0.05 were considered statistically significant in both analyses.

Detailed data on physicochemical characteristics provided by the manufacturer of the AgNPs tested in the present study are shown in Table 1. TEM analysis of commercial AgNPs with diameters of 10, 60, and 100 nm was conducted to confirm primary particle size distribution and general morphology. All of the tested AgNPs were spherical in shape (Fig. 1A), and their diameter distributions were narrow (Table 1). Changes in size, shape, and the presence of aggregates were investigated with UV-visible spectroscopy measurements (Fig. 1B). Absorption in the 600–800 nm range, which is typical for aggregates, was not detected in AgNPs, demonstrating that the presence of stable aggregates in these samples could be excluded.

One mouse in the 100 nm AgNP group at 3 h exhibited a sharp decrease in rectal temperature, accumulation of ascites fluid, and petechial hemorrhage in the intestine. Since we inferred that these findings were due to accidental injection into the intestine, the data from this animal were excluded from the results. Mice treated with 10 nm AgNPs showed piloerection and a marked decrease in activity from 5 h after treatment, but no mortality was observed for any of the mice administered AgNPs during the 6-h observation period. The body temperatures of mice treated with AgNPs, except for 60 nm AgNPs, were significantly decreased compared with those of the vehicle control (Fig. 2).

Data obtained from serum biochemistry analyses are shown in Table 2. In the 10 nm AgNP group, several significant changes in parameters were observed at 6 h. In contrast, in the 60 and 100 nm AgNP groups, most of the differences in parameters detected at 1 and 3 h were not detectable at 6 h. At 1 h post administration, decreases in BUN and Na were observed in all AgNP groups, and increased glucose was observed in the 60 nm AgNP group. At 3 h post administration, decreases were observed in BUN and TG in the 10 nm AgNP group, in BUN in the 60 nm AgNP group, and in TG in the 100 nm AgNP group, and increases were observed in IP in all AgNP groups and in glucose in the 10 nm AgNP group. At 6 h post administration, increases were observed in IP, AST, and Bil, and decreases were observed in TP, ALB, TC, TG, and glucose in the 10 nm AgNP group and in TG in the 60 nm AgNP group. Additionally, the average ALT level was obviously increased in the 10 nm AgNP group at 6 h, although this difference was not statistically significant. Since the data of the control group were analyzed only at 6 h post administration, some parameters of AgNP groups analyzed at 1 or 3 h post administration may be improper to compare with those of the control group, e.g., glucose showing circadian variation.

At autopsy, black residue of AgNPs were absorbed in the abdominal cavity in all AgNP-treated mice, and black-

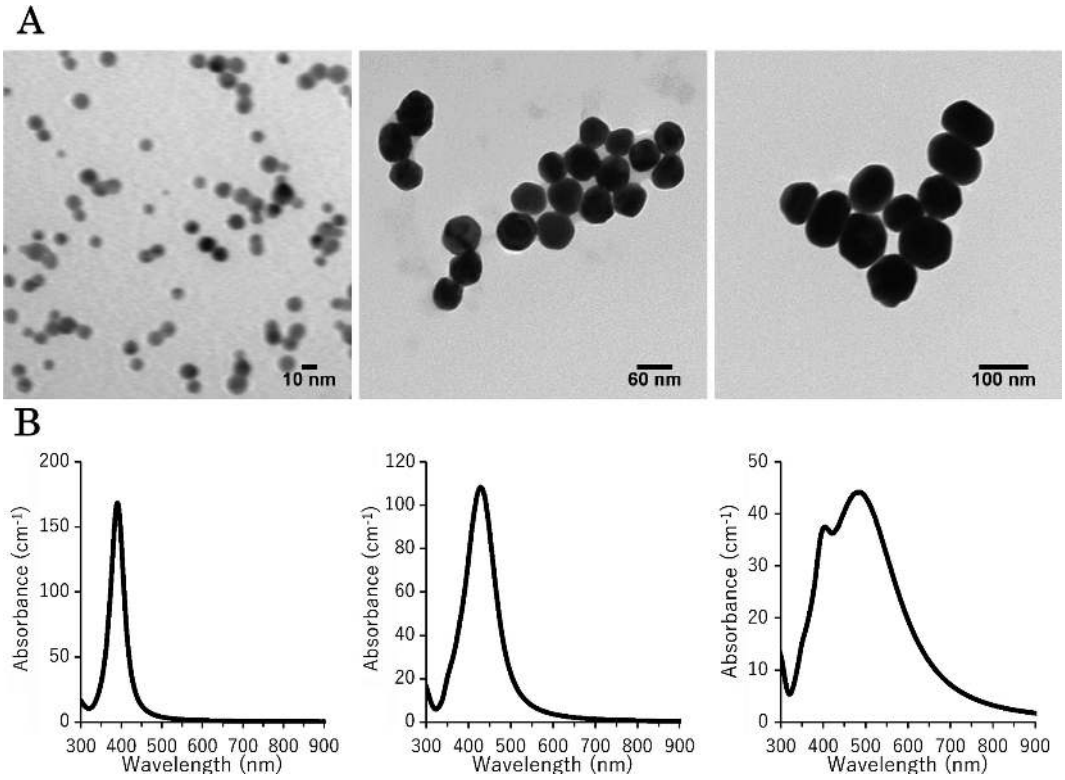

Fig. 1. TEM images (A) and UV-visible spectroscopy measurements (B) of the AgNPs used in the present study. The TEM images and UV-visible spectroscopy measurements demonstrate that each particle exhibited a spherical shape, narrow size distribution, and no stable aggregates.

colored lymph nodes were observed in the pulmonary cavity in the mice. A summary of the histopathological results is shown in Table 3. Figure 3 shows the representative histopathological findings of 10 nm AgNP-treated mice at 6 h (A–D), 60 nm AgNP-treated mice at 1 h (E), and 100 nm AgNP-treated mice at 6 h (F). Significant increases in congestion, hepatocyte vacuolation, cytoplasmic inclusions, and single cell necrosis in the liver (Fig. 3A), in congestion in the red pulp of the spleen, and in apoptosis in the white pulp of the spleen (Fig. 3B) were observed in the 10 nm AgNP group at 6 h. The incidence of apoptosis in the thymus cortex was significantly increased in the 10 nm AgNP group at 6 h and the 60 nm AgNP group at 3 h. Dark brown pigment deposition in Kupffer cells in the liver was increased in the 10 nm AgNP group at 6 h, although the difference was not significant (Fig. 3A). The pigments observed in Kupffer cells, lymph nodes, and lungs were stained by Schmorl's technique but were negative in Periodic Acid-Schiff (PAS) and autofluorescence under ultraviolet light, suggesting that the pigments were injected AgNP. Pigments showing the same staining properties were reported in Kupffer cells in the liver of DCI mice intravenously treated with Nanogold for 14 or 90 days[15]. Mitosis in the liver was significantly increased in the 60 nm AgNP group at 1 and 3 h and in the 100 nm AgNP group at 1 h (Fig. 4). Indeed, the numbers of Ki-67-positive cells in the 60 nm AgNP group at 1 h were significantly increased as compared with those of the vehicle control (Fig. 4A). The animals in the 60 nm AgNP group at 3 h and the 100 nm AgNP group at 1 and 3 h groups also showed a tendency to exhibit a higher number of positive cells than animals in the vehicle control. Ki-67-positive cells were observed mainly in the midlobular zone of the liver lobule, but no interlobar differences were noted (Fig. 4B). Submucosal edema and dilatation in the gall bladder were detected only in the AgNP-treated group (Fig. 3C). In all treated groups, increases in inflammatory cell foci and dark brown pigment deposition were found in the mesentery (Fig. 3F), and similar pigment deposition was observed in the thoracic lymph nodes (mainly in the medullary sinus and subcapsular sinus; Fig. 3D). Inflammatory cell foci containing dark brown pigment in the mesentery were mainly observed distant from the mesenteric lymph node, in which lymphocytes and macrophages were predominant (Fig. 3F). Although the differences were not significant, hemorrhage

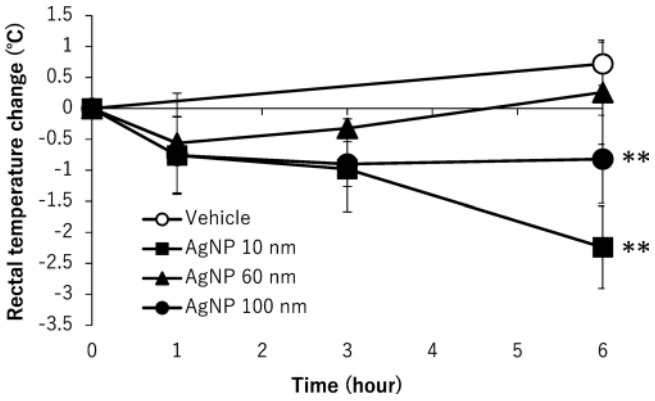

Fig. 2. Changes in the rectal temperatures of mice after intraperitoneal administration of 10, 60, and 100 nm AgNPs. Rectal temperatures were measured with a rectal thermometer just before injection and at 1, 3, and 6 h. The vehicle control was 2 mM citrate. Data are the means ± standard deviations (SDs) of each group (n=5 except n=4 for 100 nm AgNPs at 3 h). $^{**}P<0.01$ versus the vehicle control group.

Table 2. Serum Biochemistry in BALB/c Mice Treated with AgNPs

Treatment		Vehicle	AgNP 10 nm			AgNP 60 nm			AgNP 100 nm		
Time after treatment		6 h	1 h	3 h	6 h	1 h	3 h	6 h	1 h	3 h	6 h
No. of animals		5	5	5	5	5	5	5	5	4	5
TP	g/dL	4.78 ± 0.13	4.54 ± 0.28	4.74 ± 0.18	4.06 ± 0.17**	4.5 ± 0.21	4.7 ± 0.16	4.64 ± 0.15	4.62 ± 0.13	4.78 ± 0.26	4.58 ± 0.19
ALB	g/dL	3.30 ± 0.10	3.24 ± 0.17	3.34 ± 0.09	2.88 ± 0.08**	3.14 ± 0.15	3.28 ± 0.15	3.22 ± 0.16	3.28 ± 0.08	3.35 ± 0.13	3.14 ± 0.13
A/G		2.24 ± 0.09	2.50 ± 0.16	2.40 ± 0.19	2.44 ± 0.23	2.34 ± 0.21	2.30 ± 0.19	2.30 ± 0.33	2.46 ± 0.05	2.38 ± 0.22	2.20 ± 0.20
BUN	mg/dL	31.8 ± 4.9	19.9 ± 2.3**	22.3 ± 3.5**	27.7 ± 5.4	19.8 ± 2.1*	23.6 ± 2.9*	30.0 ± 3.6	17.0 ± 2.4**	26.6 ± 5.9	30.5 ± 1.9
Cre	mg/dL	0.13 ± 0.01	0.11 ± 0.01	0.11 ± 0.02	0.11 ± 0.02	0.12 ± 0.01	0.11 ± 0.01	0.14 ± 0.03	0.12 ± 0.01	0.12 ± 0.01	0.12 ± 0.01
Na	mEq/L	152 ± 1	147 ± 2**	151 ± 2	151 ± 2	145 ± 2*	151 ± 1	152 ± 1	148 ± 2**	152 ± 1	153 ± 2
K	mEq/L	4.68 ± 0.19	4.56 ± 0.23	4.54 ± 0.26	5.14 ± 0.29	5.06 ± 0.37	4.74 ± 0.27	5.06 ± 0.27	4.82 ± 0.29	4.65 ± 0.13	4.84 ± 0.24
Cl	mEq/L	115 ± 2	111 ± 2	110 ± 8	111 ± 7	108 ± 3	112 ± 1	114 ± 2	110 ± 2	112 ± 1	114 ± 1
Ca	mg/dL	8.20 ± 0.20	8.18 ± 0.41	7.38 ± 0.67	7.33 ± 0.22	8.22 ± 0.41	7.38 ± 0.3	7.92 ± 0.62	7.98 ± 0.48	7.78 ± 0.78	8.46 ± 0.27
IP	mg/dL	8.34 ± 0.6	9.8 ± 0.6	11.8 ± 2.4**	11.0 ± 0.7*	10.5 ± 1.1	12.8 ± 1.1*	10.3 ± 1.5	10.2 ± 1.9	11.3 ± 0.6*	9.3 ± 0.9
AST	IU/L	54.8 ± 10.5	60.2 ± 6.9	74.2 ± 34.8	348 ± 98**	60.8 ± 11.2	57.8 ± 12.6	52.0 ± 11.1	108 ± 97	52.8 ± 11.1	47.4 ± 3.8
ALT	IU/L	27.0 ± 7.2	14.6 ± 13.2	17.0 ± 4.9	54.0 ± 20.7	28.0 ± 9.3	23.8 ± 4.0	21.2 ± 5.9	56.8 ± 65.1	22.5 ± 5.8	18.6 ± 1.7
ALP	IU/L	565 ± 50	565 ± 23	607 ± 47	513 ± 47	572 ± 42	617 ± 25	574 ± 16	577 ± 73	623 ± 31	527 ± 42
γGTP	IU/L	<3	<3	<3	<3	<3	<3	<3	<3	<3	<3
TC	mg/dL	68.8 ± 3.7	64.4 ± 3.7	67.8 ± 3.6	59.0 ± 4.2**	69.0 ± 2.4	73.8 ± 6.5	69.6 ± 5.7	64.4 ± 2.5	73.5 ± 3.7	70.4 ± 3.4
TG	mg/dL	60.2 ± 19.8	44.2 ± 11.8	28.6 ± 8.7**	19.0 ± 5.2**	68.2 ± 7.4	41.6 ± 10.6	34.6 ± 9.0*	49.6 ± 8.7	38.0 ± 9.1*	49.2 ± 17.5
BIL	mg/dL	0.04 ± 0	0.07 ± 0.01	0.12 ± 0.14	0.14 ± 0.02*	0.09 ± 0.04	0.08 ± 0.04	0.05 ± 0.02	0.09 ± 0.06	0.06 ± 0.01	0.05 ± 0
Glucose	mg/dL	162 ± 16	221 ± 22	203 ± 27**	111 ± 19*	216 ± 22*	197 ± 33	143 ± 21	194 ± 30	176 ± 38	146 ± 15

Values represent means ± SDs. *Significantly different from vehicle group ($P<0.05$). **Significantly different from vehicle group ($P<0.01$).

(Fig. 3E) and neutrophil infiltration were observed in the lung in the 60 nm AgNP group at 1 h, and thrombus was observed in the heart in the 10 nm AgNP group at 1 h. Other lesions were sporadically detected, but no significant differences were observed.

In the present study, mice administered 10 nm AgNPs showed reduced activity and piloerection at 5 h post administration, and lowered body temperatures were observed at 6 h post administration were observed with histopathological changes of congestion, vacuolation, and single cell necrosis in the liver; congestion in the spleen; and apoptosis in the thymus cortex at 6 h post administration. These histopathological changes were not evident following administration of either 60 or 100 nm AgNPs.

The AgNPs used in the present study were thoroughly characterized by the manufacturer before our investigation of their toxicological effects *in vivo*. *In vitro*, the toxicity of these particles varies, from high cytotoxicity (0.2 μg/mL)[16] to almost no cytotoxicity (up to 1.7 μg/mL)[17]. Because of the apparent conflicting results with regard to the cytotoxicity of AgNPs, which may partly reflect differences among the studies in the type of AgNPs tested (size, coating, sur-

Table 3. Histopathological Findings in BALB/c Mice Treated with AgNPs

	Treatment	Vehicle	AgNP 10 nm			AgNP 60 nm			AgNP 100 nm		
Organ and lesions	Time after treatment	6 h	1 h	3 h	6 h	1 h	3 h	6 h	1 h	3 h	6 h
	No. of animals	5	5	5	5	5	5	5	5	4	5
Liver	Congestion	0	0	0	5**	0	0	0	0	0	0
	Vacuolation, hepatocyte	0	0	0	5**	0	0	0	0	0	0
	Cytoplasmic inclusions, hepatocyte	0	0	0	5**	0	1	0	0	0	0
	Single cell necrosis, hepatocyte	0	0	0	5**	1	0	0	0	0	0
	Focal necrosis, hepatocyte	0	0	0	3	0	0	1	2	1	0
	Mitosis, hepatocyte	0	1	0	0	5**	5**	2	5**	2	1
	Megalocyte, hepatocyte	0	0	0	0	1	1	0	1	0	0
	Dark brown pigment deposition, Kupffer cell	0	0	0	3	0	0	0	0	0	0
	Infiltration, neutrophil	0	0	0	0	1	0	0	0	0	0
	Hyperplasia, mesothelium	0	0	0	1	0	0	0	0	0	0
Gall bladder	Edema, submucous	0	3	2	5**	5**	4*	0	3	2	2
	Edema, subserosa	0	0	1	2	0	0	0	0	0	0
	Dilatation	0	4*	1	5**	2	2	2	4*	2	0
	Vacuolation, epithelium	0	0	1	0	0	0	0	0	0	0
	Cell infiltration, submucous, lymphocytic	0	0	0	0	0	1	0	0	0	0
Spleen	Congestion	0	0	0	4*	0	0	0	0	0	0
	Apoptosis, white pulp	0	0	0	2	1	0	1	3	3	1
	Extramedullary hematopoiesis, erythrocytic	0	1	1	1	0	0	0	0	0	0
Thymus	Apoptosis, cortex	0	0	3	5**	2	4*	1	0	3	0
	Apoptosis, medulla	0	0	1	1	0	1	0	0	0	0
Thoracic lymph node	Dark brown pigment deposition, lymphocyte	0	3	5**	5**	4*	3	4*	3	3	3
	Congestion	0	0	0	1	0	0	0	1	0	0
Intestine	Hemorrhage, large intestine, submucous	0	0	0	1	0	0	0	0	0	0
	Congestion, large intestine, lamina propria	0	0	0	1	0	0	0	0	0	0
	Vacuolation, small intestine, mucosal epithelium	0	0	0	1	0	0	0	0	0	0
	Small intestine injection track	0	0	0	0	0	1	0	0	0	0
	Cecum injection track	0	0	0	0	0	0	0	0	1	0
Mesenterium	Inflammatory cells foci	0	3	4*	5**	5**	5**	5**	5**	4	5**
	Dark brown pigment deposition	0	3	5**	5**	5**	5**	5**	5**	4	5**
	Erythrophagocytosis	0	0	1	1	1	0	1	0	0	0
Mesenteric lymph nodes	Apoptosis, cortex	0	1	2	3	2	4*	2	0	4*	2
	Apoptosis, paracortex	0	2	3	3	1	2	2	2	1	3
Kidney	Regenerative tubules	4	5	5	5	5	5	3	5	5	5
	Mineralization, medulla	0	0	0	0	0	0	1	0	0	0
	Cell infiltration, interstitial, lymphocytic	0	0	0	0	0	1	0	0	0	0
Heart	Thrombus, right atrium	0	1	0	0	0	0	0	0	0	0
	Mineralization, epicardium	4	5	2	4	3	2	3	3	1	2
	Mineralization, myocardium	0	0	0	0	1	0	0	0	0	0
	Mineralization, endocardium	0	0	0	1	0	0	0	0	0	0
	Cell infiltration, interstitial, lymphocytic	0	0	1	0	0	0	1	0	0	0
	Cell infiltration, interstitial, neutrophil	0	0	0	0	0	0	1	0	0	0
Lung	Hemorrhage	0	0	0	0	1	0	0	0	0	0
	Cell infiltration, interstitial, neutrophil	0	0	0	0	1	0	0	0	0	0
	Dark brown pigment deposition, alveolar macrophage	0	0	0	1	1	0	0	1	0	0
	Lymphatic hyperplasia	0	0	0	1	0	0	0	1	0	0

*Significantly different from vehicle group ($P<0.05$). **Significantly different from vehicle group ($P<0.01$).

face charge, solubility), cell type, and the technique used for exposing the cells, such as the dispersion method (dispersing agent, sonication, agglomeration), rigorous characterization of the AgNPs is necessary to produce data that can help provide scientific answers to regulatory issues for widely used AgNPs. AgNPs having a narrow size range are advantageous for analysis of the effects of size on toxicity. Although the mass concentration (mg/mL) was the same, 10 nm AgNPs have surface areas and particle concentrations (number/mL) that are over 10- and 1,000-times larger than those of 100 nm AgNPs, respectively, which may increase the chance of interaction with surrounding biomolecules and, as a consequence, trigger adverse responses. In cytotoxicity assays measuring membrane damage with human lung cells, 20 and 50 μg/mL AgNPs measuring 10 nm in diameter, independent of the surface coating (citrate and polyvinylpyrrolidone [PVP]), were found to be toxic, whereas 40 and 75 nm NPs were not[7]. Similarly, 4 nm AgNPs were found to induce much higher levels of reactive oxygen species (ROS) production and interleukin-8 secretion from

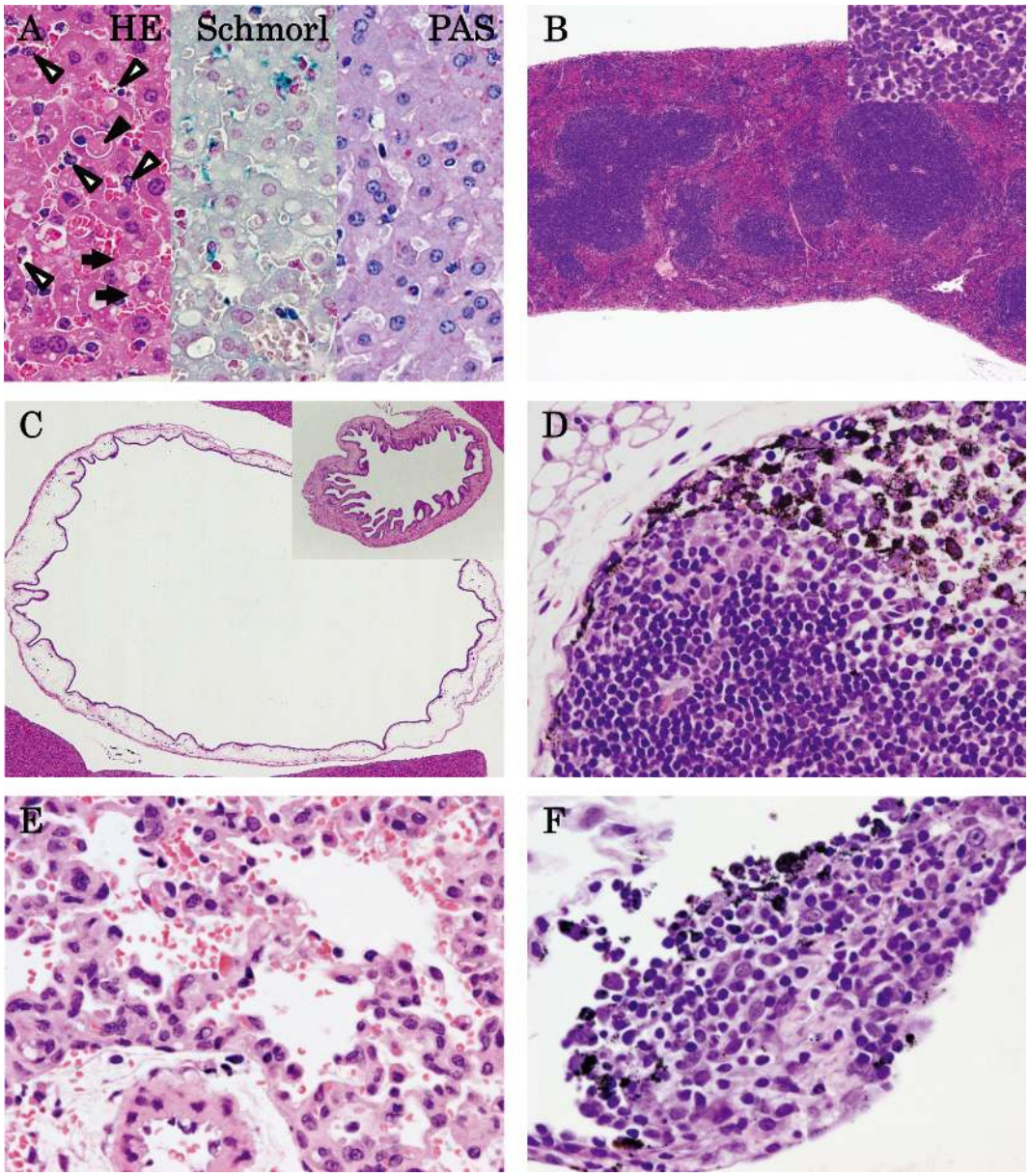

Fig. 3. Histopathology of 10 nm AgNPs at 6 h (A–D) post administration, 60 nm AgNPs at 1 h (E) post administration, and 100 nm AgNPs at 6 h (F) post administration. (A) Congestion in the liver, hepatocyte vacuolation and dark brown pigment deposition in Kupffer cells (open arrowhead), hepatocyte single cell necrosis (closed arrowhead), and inclusion bodies in cytoplasm (arrow) were observed in HE staining; a slightly blue reaction of pigments was observed with Schmorl's stain, but the results were negative with PAS stain (×400). (B) Congestion in the red pulp and apoptosis in the white pulp of the spleen (insert; ×40). (C) Submucosal edema and dilatation in the gall bladder (insert, control; ×40). (D) Dark brown pigment deposition in the medullary sinus and subcapsular sinus of the thoracic lymph node (×400). (E) Hemorrhage in the lung (×400). (F) Dark brown pigment deposition in inflammatory cell foci of the mesenterium (×400).

macrophage immune cells than 20 and 70 nm AgNPs[18], suggesting that the sizes of the particles may be the principle factor affecting the toxicity of AgNPs.

Elkhawass *et al.* reported that mice intraperitoneally treated with a single dose of 214 mg/kg bw 20 nm AgNPs showed more severe symptoms of passive behavior, piloerection, labored breathing, impaired movement, arching of the back, loss of appetite, diarrhea, and death than the mice treated with 448 mg/kg bw 50 nm AgNPs until day 14, suggesting that systemic symptoms are also related to the size of AgNPs[14]. The dose volume applied in the present study (9.9–12.3 mg/kg bw) was obviously lower than that in the report by Elkhawass *et al.* (214 mg/kg bw)[14], in which histopathological analysis was not performed. In the present study, the results of histopathological, including congestion in the liver and the spleen and thrombus in the heart, suggested that life-threatening toxicity may be partially caused by circulatory failure.

A significant increase in AST and an increasing tendency in ALT were observed in the 10 nm AgNP group in the present study. These findings are consistent with a previous study in male Sprague-Dawley rats, in which an increase in AST and ALT or AST only was observed after a single oral administration of Ag ions (20 mg/kg) or 7.9 nm AgNPs (2 or 20 mg/kg), respectively[19]. The greatest accumulation of Ag content in animals exposed by the intravenous, oral, intraperitoneal, and subcutaneous routes was in the liver, followed by the spleen, kidney, and brain[12, 14, 20–22]. Even in inhalation toxicity studies, Ag content was observed in the liver, kidneys, olfactory bulb, brain, and blood in addition to the lungs[11]. Thus, the liver may be the main target of AgNPs. The organs and tissues in which intraperitoneally administered AgNPs seemed to be absorbed and accumulated were consistent with those showing lesions in the present study. The different incidences of lesions in the liver in the 60 and 100 nm AgNP groups may be due to lower uptake or ROS generation rates than those in the 10 nm AgNP group. High reactivity and easy transportability into the cell may lead to such high toxicity for small NPs[18].

In the present study, increased mitosis in the liver was noted in the 60 and 100 nm AgNP groups, but not in the 10 nm AgNP group, at early time points. The toxic potencies of 60 and 100 nm AgNPs are obviously weaker than that of 10 nm AgNP under the condition adjusted by silver concentration. A stimulating effect in which low concentrations of AgNPs accelerate proliferation was reported in mouse embryonic stem cells[23] and HepG2 cells[24]. Taken together, potentially toxic agents might induce cell proliferation rather than cytotoxicity at low levels. Apoptosis in the thymus was observed only in the 10 nm AgNP group; this effect was thought to be related to stress because there was clear evidence of other stress-related phenomena, such as inactivation, piloerection, and low body temperature.

The potential molecular mechanisms of AgNP toxicity have been studied in human ovarian cancer cell lines and human colon cancer cell lines. Briefly, AgNPs with a diameter of 7.5 nm can interact with membrane proteins and activate signaling pathways, leading to inhibition of cell proliferation[25]. AgNPs (<100 nm) were shown to enter human lung epithelial cells through diffusion or endocytosis to cause generation of ROS, leading to damage to proteins and nucleic acids and ultimately inhibition of cell proliferation[26].

In conclusion, small citrate-stabilized AgNPs with a narrow size range (e.g., 10 nm in diameter) were found to elicit significantly higher acute toxicity in mice following intraperitoneal administration.

Disclosure of Potential Conflicts of Interest: The authors declare that there are no conflicts of interest associated with this manuscript.

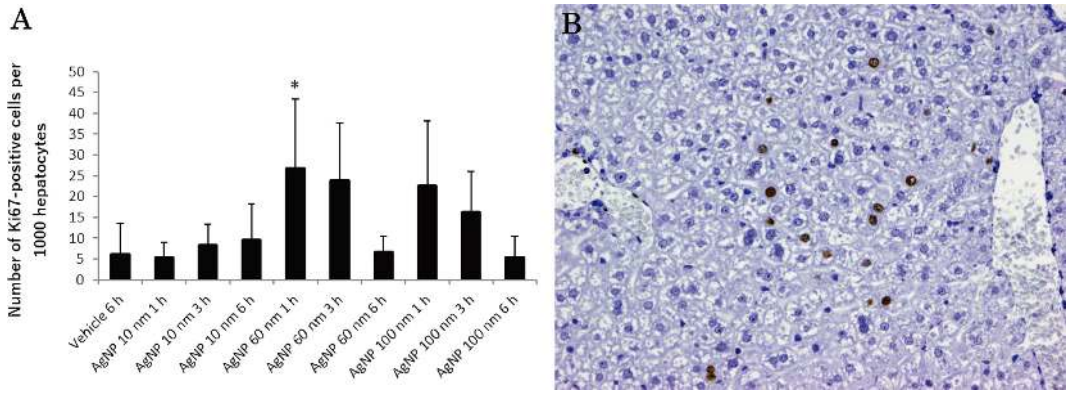

Fig. 4. Evaluation of Ki-67-positive cells in the liver. (A) The graphs show positive cells per 1,000 hepatocytes in the vehicle control at 6 h; 10 nm AgNP group at 1 h, 3 h, and 6 h; 60 nm AgNP group at 1 h, 3 h, and 6 h; and 100 nm AgNP group at 1 h, 3 h, and 6 h. Ki-67-positive cells in the 60 nm AgNP group at 1 h were significantly increased as compared with those of the vehicle control. Data are the means ± standard deviations (SDs) of each group (n=5 except n=4 for 100 nm AgNPs at 3 h). **P*<0.05 versus the vehicle control group. (B) Photomicrographs show the distribution of Ki-67-positive cells in the liver of the 60 nm AgNP group at 1 h. Ki-67-positive cells were observed mainly in the midlobular zone of the liver lobule (×200).

Acknowledgments: We thank Ms. Ayako Saikawa and Ms. Yoshimi Komatsu for their expert technical assistance with the processing of histological materials. This work was supported by a Grant-in-Aid from the Ministry of Health, Labour and Welfare, Japan.

References

1. Quang Huy T, Van Quy N, and Anh-Tuan L. Silver nanoparticles: synthesis, properties, toxicology, applications and perspectives. Advances in Natural Sciences: Nanoscience and Nanotechnology. **4**: 1–20. 2013.
2. Panacek A, Kvítek L, Prucek R, Kolar M, Vecerova R, Pizúrova N, Sharma VK, Nevecna T, and Zboril R. Silver colloid nanoparticles: synthesis, characterization, and their antibacterial activity. J Phys Chem B. **110**: 16248–16253. 2006. [Medline] [CrossRef]
3. Rai M, Yadav A, and Gade A. Silver nanoparticles as a new generation of antimicrobials. Biotechnol Adv. **27**: 76–83. 2009. [Medline] [CrossRef]
4. Mikklesen HS, Hansen E, Christensen TB, Baun A, Hansen FS, and Binderup M-L. Survey on basic knowledge about exposure and potential environmental and health risks for selected nanomaterials. 2011, from DEPA website: http://www2.mst.dk/udgiv/publications/2011/08/978–87–92779–09–0.pdf.
5. Vance ME, Kuiken T, Vejerano EP, McGinnis SP, Hochella MF Jr, Rejeski D, and Hull MS. Nanotechnology in the real world: Redeveloping the nanomaterial consumer products inventory. Beilstein J Nanotechnol. **6**: 1769–1780. 2015. [Medline] [CrossRef]
6. Majdalawieh A, Kanan MC, El-Kadri O, and Kanan SM. Recent advances in gold and silver nanoparticles: synthesis and applications. J Nanosci Nanotechnol. **14**: 4757–4780. 2014. [Medline] [CrossRef]
7. Gliga AR, Skoglund S, Wallinder IO, Fadeel B, and Karlsson HL. Size-dependent cytotoxicity of silver nanoparticles in human lung cells: the role of cellular uptake, agglomeration and Ag release. Part Fibre Toxicol. **11**: 11. 2014. [Medline] [CrossRef]
8. Hackenberg S, Scherzed A, Kessler M, Hummel S, Technau A, Froelich K, Ginzkey C, Koehler C, Hagen R, and Kleinsasser N. Silver nanoparticles: evaluation of DNA damage, toxicity and functional impairment in human mesenchymal stem cells. Toxicol Lett. **201**: 27–33. 2011. [Medline] [CrossRef]
9. Lu W, Senapati D, Wang S, Tovmachenko O, Singh AK, Yu H, and Ray PC. Effect of surface coating on the toxicity of silver nanomaterials on human skin keratinocytes. Chem Phys Lett. **487**: 92–96. 2010. [Medline] [CrossRef]
10. Singh RP, and Ramarao P. Cellular uptake, intracellular trafficking and cytotoxicity of silver nanoparticles. Toxicol Lett. **213**: 249–259. 2012. [Medline] [CrossRef]
11. Sung JH, Ji JH, Park JD, Yoon JU, Kim DS, Jeon KS, Song MY, Jeong J, Han BS, Han JH, Chung YH, Chang HK, Lee JH, Cho MH, Kelman BJ, and Yu IJ. Subchronic inhalation toxicity of silver nanoparticles. Toxicol Sci. **108**: 452–461. 2009. [Medline] [CrossRef]
12. Kim YS, Song MY, Park JD, Song KS, Ryu HR, Chung YH, Chang HK, Lee JH, Oh KH, Kelman BJ, Hwang IK, and Yu IJ. Subchronic oral toxicity of silver nanoparticles. Part Fibre Toxicol. **7**: 20. 2010. [Medline] [CrossRef]
13. Kim JS, Song KS, Sung JH, Ryu HR, Choi BG, Cho HS, Lee JK, and Yu IJ. Genotoxicity, acute oral and dermal toxicity, eye and dermal irritation and corrosion and skin sensitisation evaluation of silver nanoparticles. Nanotoxicology. **7**: 953–960. 2013. [Medline] [CrossRef]
14. Elkhawass EA, Mohallal ME, and Soliman MFM. Acute toxicity of different sizes of silver nanoparticles intraperitonally injected in Balb/C mice using two toxicological methods. Int J Pharm Pharm Sci. **7**: 94–99. 2014.
15. You J, Zhou J, Zhou M, Liu Y, Robertson JD, Liang D, Van Pelt C, and Li C. Pharmacokinetics, clearance, and biosafety of polyethylene glycol-coated hollow gold nanospheres. Part Fibre Toxicol. **11**: 26. 2014. [Medline] [CrossRef]
16. Park MV, Neigh AM, Vermeulen JP, de la Fonteyne LJ, Verharen HW, Briedé JJ, van Loveren H, and de Jong WH. The effect of particle size on the cytotoxicity, inflammation, developmental toxicity and genotoxicity of silver nanoparticles. Biomaterials. **32**: 9810–9817. 2011. [Medline] [CrossRef]
17. Samberg ME, Oldenburg SJ, and Monteiro-Riviere NA. Evaluation of silver nanoparticle toxicity in skin in vivo and keratinocytes in vitro. Environ Health Perspect. **118**: 407–413. 2010. [Medline] [CrossRef]
18. Park J, Lim DH, Lim HJ, Kwon T, Choi JS, Jeong S, Choi IH, and Cheon J. Size dependent macrophage responses and toxicological effects of Ag nanoparticles. Chem Commun (Camb). **47**: 4382–4384. 2011. [Medline] [CrossRef]
19. Park K. Toxicokinetic differences and toxicities of silver nanoparticles and silver ions in rats after single oral administration. J Toxicol Environ Health A. **76**: 1246–1260. 2013. [Medline] [CrossRef]
20. Lankveld DP, Oomen AG, Krystek P, Neigh A, Troost-de Jong A, Noorlander CW, Van Eijkeren JC, Geertsma RE, and De Jong WH. The kinetics of the tissue distribution of silver nanoparticles of different sizes. Biomaterials. **31**: 8350–8361. 2010. [Medline] [CrossRef]
21. Park K, Park EJ, Chun IK, Choi K, Lee SH, Yoon J, and Lee BC. Bioavailability and toxicokinetics of citrate-coated silver nanoparticles in rats. Arch Pharm Res. **34**: 153–158. 2011. [Medline] [CrossRef]
22. Tang J, Xiong L, Wang S, Wang J, Liu L, Li J, Yuan F, and Xi T. Distribution, translocation and accumulation of silver nanoparticles in rats. J Nanosci Nanotechnol. **9**: 4924–4932. 2009. [Medline] [CrossRef]
23. Gao X, Topping VD, Keltner Z, Sprando RL, and Yourick JJ. Toxicity of nano- and ionic silver to embryonic stem cells: a comparative toxicogenomic study. J Nanobiotechnology. **15**: 31. 2017. [Medline] [CrossRef]
24. Kawata K, Osawa M, and Okabe S. In vitro toxicity of silver nanoparticles at noncytotoxic doses to HepG2 human hepatoma cells. Environ Sci Technol. **43**: 6046–6051. 2009. [Medline] [CrossRef]
25. Kang SJ, Ryoo IG, Lee YJ, and Kwak MK. Role of the Nrf2-heme oxygenase-1 pathway in silver nanoparticle-mediated cytotoxicity. Toxicol Appl Pharmacol. **258**: 89–98. 2012. [Medline] [CrossRef]
26. Suliman Y AO, Ali D, Alarifi S, Harrath AH, Mansour L, and Alwasel SH. Evaluation of cytotoxic, oxidative stress, proinflammatory and genotoxic effect of silver nanoparticles in human lung epithelial cells. Environ Toxicol. **30**: 149–160. 2015. [Medline] [CrossRef]